2012

Effect of Louver Angle on Performance of Heat Exchanger With Serpentine Fins and Flat Tubes in Periodic Frosting

Predrag S. Hrnjak
pega@illinois.edu

Ping Zhang

Chris Rennels

Effect of louver angle on performance of heat exchanger with serpentine fins and flat tubes in frosting

Pega Hrnjak[1,3 *], Ping Zhang[1,2], Chris Rennels[1]

[1]University of Illinois, Department of Mechanical Science and Engineering ACRC, Urbana, IL, USA
also [3]Creative Thermal Solutions, Inc. Urbana, IL, USA
[2]Zhejiang Vocational College of Commerce, Hangzhou, Binwen Road 470, China
E-mail: pega@illinois.edu

ABSTRACT

This paper presents the results of an experimental study on the air-side pressure drop and overall heat transfer coefficient characteristics for serpentine-louvered-fin, microchannel heat exchanger in periodic frosting. It focuses on quantification of the effects of louver angle on heat transfer and pressure drop and on defrost and refrost times. Nine heat exchangers differing in louver angle and fin pitch (i.e. louver angle 15º to 39º and fin pitch 15 to 18 fpi) are studied. The face velocity was 3.5 ms/ and inlet air relative humidity of 70% and 80%. Effect of fin pitch and louver pitch on initial Colburn j0 factor and Fanning friction f0 factor during the start of the first frosting cycle are reported, and compared to the prediction by the Chang and Wang (1997).

1. INTRODUCTION

Microchannel heat exchangers are becoming quite popular as a compact alternative to bulkier fin-and-tube heat exchangers when used mostly as condensers. Charge reduction is an additional benefit. However, microchannel heat exchangers are still not widely used as outdoor coil in heat pump systems. Special concerns are related to condensate removal, drainage, in the dehumidification mode and in defrosting, besides refrigerant distribution that is not object of this paper.

It is well accepted that louver directed flow is important for increase in heat transfer coefficient since Achaichia and Cowell (1988) and later other publications. In addition to conventional deterioration effects frost buildup on the louvers strongly affects air-side performance by altering the flow from louver directed flow to duct directed flow. Thus, to identify geometry that will be more frost tolerant and quantify effects, it is important to shed more light on the effects of the geometrical parameters on the air flow during frosting.

Several studies of frost properties and frost growth mechanism on the round-tube-plate-fin heat exchanger have been reported. Kondepudi and O'Neal (1987) reviewed the literature on the effect of frost formation on finned tube heat exchanger performance, and Kondepudi and O'Neal (1989) conducted frost growth research on louver-fin-round-tube heat exchangers. Machielsen and Kerschbaumer (1989) conducted research on the effects of frosting and defrosting on heat exchanger performance. Yan et al. (2005) investigated the performance of frosted finned-tube heat exchangers with plain fins, single-bank louvered fins, and multi-louvered fins, and found that the heat transfer rate, the overall heat transfer coefficient, and the pressure drop for multi-louvered fins were higher than for others.

Only a few studies dealing with the effects of frost on the flat tube louvered compact heat exchanger have been published in the open literature to date. Kim and Groll (2003) reported a comparison between microchannel and fin-tube heat exchangers when used as an outdoor coil in a heat pump system. The study included both cooling and heating tests. The authors reported frosting/defrosting time and the heating capacity of the heat pump with both coils. The effects of other variables such as heat exchanger inclination and fins per inch were also studied. The authors concluded that microchannel heat exchangers have a shorter frosting time compared to fin-tube heat exchangers and that the frosting time decreased even further with each cycle due to residual water retained at the end of each defrost cycle. Xia et al. (2006) studied the effects of frost, defrost, and refrost on the air-side thermal-hydraulic performance of louvered-fin, flat tube heat exchanger which resembled a microchannel heat exchanger. An overall heat transfer coefficient was obtained for the heat exchanger for a realistic range of temperatures and flow rates. Frost thickness was measured using images captured with a CCD camera and frost weight was obtained by using a high precision scale. They developed a numerical model, which was also experimentally validated, to predict the frost thickness and blockage ratio. Additional studies include Carlson and Hrnjak [2001] who focused on understanding how environmental conditions, air temperature and relative humidity, refrigerant temperature, and air and refrigerant temperature glide, affect the deposition and distribution of frost on heat exchangers, specifically of

those found in refrigerated display cases. Sankar Padhmanabhan et al [2008] compared frost and defrost cycling performance between a microchannel heat exchanger with louvered fin and a fin-tube heat exchanger with straight fins employed as outdoor coils of a heat pump system. Local surface temperature and weight of the coil were taken in real time during the experiment. The mass of frost accumulation during heating tests was obtained by using load cells. Zhang and Hrnjak (2009, 2010a, 2010b) analyzed and compared air-side performance of three types of heat exchanges in frosting conditions. They studied effect of some geometric parameters on performance of PF2 heat exchanger in periodic frosting and compared to serpentine louvered fin geometry.

However, there is very little has been published to address frost formation and defrosting on serpentine-louvered-fin heat exchanger and little basis available in the open literature for the design of microchannel heat exchanger. This paper measured the effect of louver angle on the air-side heat exchanger performance in a range of typical operating conditions in search for good value of louver angle parameter. In addition authors hope that this study will provide additional insights into the performance of microchannel heat exchangers under cyclical frosting conditions.

2. EXPERIMENTAL FACILITY AND PROCEDURE

The experimental facility used to test the heat exchangers is shown in Figure 1. A single phase secondary refrigerant, 100% ethyl alcohol, is cooled by an R404A chiller system and pumped through the experimental loop. The alcohol mass flow rate is controlled by adjusting the pump speed. A Coriolis-effect mass flow meter (±0.1%, range: 0-2180kg/h) is used to measure the mass flow rate through the heat exchanger. The alcohol temperature is controlled using PID1 to regulate power supplied to Heater 1 and is measured using immersion thermocouple probes (±0.2°C) at the inlet and exit of the heat exchanger.

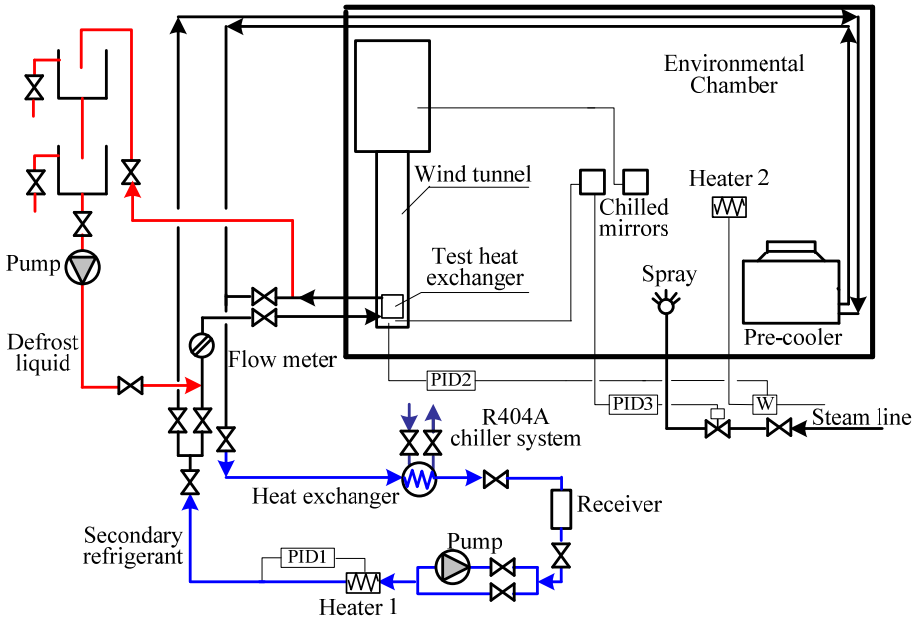

Figure 1: Experimental facility

The environmental chamber houses a pre-cooler, heater, steam inlet, two chilled-mirror sensors, and the wind tunnel. The pre-cooler is used to cool the chamber to the test conditions. A 3.2 kW heater (Heater 2) is used to maintain a constant air temperature within the chamber, balancing the cooling effect of the pre-cooler. It is connected to PID2, which controls the test heat exchanger air inlet temperature based on a reading of a type-T thermocouple (±0.2°C) placed near the entrance to the heat exchanger. Steam is used to maintain a constant dew point within the environmental test chamber. It goes through a manually adjusted valve and then a solenoid valve, which is opened and closed by using PID3, controlled by a General Eastern model D-2-SR chilled-mirror dew-point sensor (±0.2°C). Two chilled-mirror sensors of the same model are used to measure dew points upstream and downstream of the test heat exchanger.

The wind tunnel consists of a plexiglass section, duct section, and a blower (Figure 2). The test heat exchanger is placed in the plexiglass section so observation from the side is possible. The plexiglass section also acts as an airflow straightener by utilizing wire mesh in the necessary positions because of the great aspect ratio of the duct. A

nozzle is located in the duct section to measure the air mass flow rate. Three pressure taps are placed at the downstream side of the heat exchanger and four pressure taps are placed at both sides of the nozzles. Pressure differences across the nozzle and test heat exchanger are measured by pressure transducers Setra model 239 (±0.14% FS, range: 0-249). The blower used during the tests runs at a constant speed throughout all experiments.
Air temperatures are measured using two grids of thermocouples at the inlet and outlet of the heat exchanger. Calibration provides accuracy of ±0.2 K.

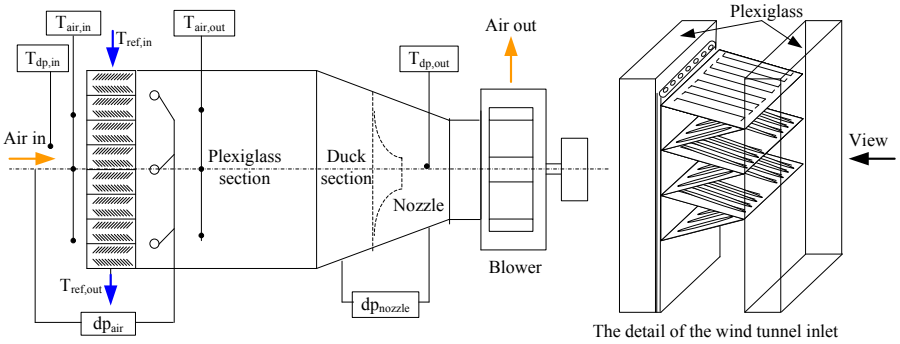

Figure 2: The open wind tunnel inside the environmental chamber

Table 1
Test conditions

$T_{a,in}$ [°C]	$T_{r,in}$ [°C]	ϕ [%]	υ [m s^{-1}]	t_d [min]	T_d [°C]	dP_a kPa
0	-11	70%; 80%	3.5	2	20	$5\,dP_0$

The data logger sampled values at 10s intervals, and six measurements are averaged to provide the results in 1min intervals. The data are written into a text file for subsequent analysis.
The experiments are conducted at constant: air-inlet temperature, refrigerant-inlet temperature, air inlet humidity, refrigerant mass flow rate, and air flow rate. The test conditions are given in Table 1. Prior to taking data, alcohol flows only to the pre-cooler until the chamber is cooled to the desired temperature. Once the test condition is reached, the experiment is initiated; the secondary refrigerant flows to the test heat exchanger and data collection begins. When the air-side pressure drop across the test heat exchanger increases to five times its initial value, the defrost cycle is initiated and the secondary refrigerant at 20°C is pumped through the heat exchanger to melt the frost. After defrost, valves are switched and the refrigeration cycle begins. The system goes through multiple cycles of defrost and refrost.

3. THE GEOMETRY OF HEAT EXCHANGERS EXPLORED

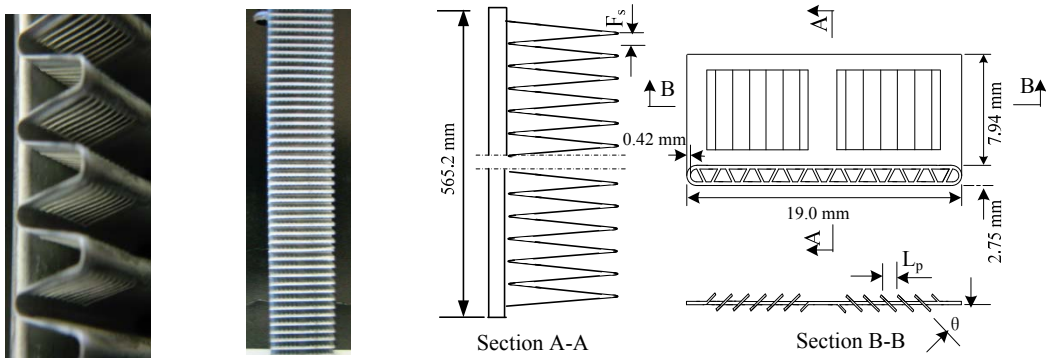

Figure 3: Structure of the test heat exchanger

Fig. 3 indicates geometrical configuration and terminology of the test heat exchanger. The heat exchangers are multi-louvered fin and flat tube heat exchangers. Total of nine heat exchanger samples are used for the test. Table 2 shows specification of the test heat exchangers. The geometrical differences between these heat exchangers are the fin pitch (12 fpi to 18 fpi) and louver angle (15º to 39º): see Table 1. The test heat exchangers consist of one microchannel tube brazed to one row of louvered fins as shown in Figure 3. A sheet of plexiglass is used in place of the second tube in order to photograph the heat exchanger during the frosting and refrosting periods. A CCD camera was used to visually capture the frosting, defrosting and refrosting processes and to help explain the reasoning behind the differences between heat exchanger performances. The airflow and the tube are vertical plane, with refrigerant entering from the top and leaving at the bottom.

Table 2:
Sample geometries (B1, B2 and B3 presented in this paper)

HX Name	F_p / F_s [fpi]/[mm]	L_p [mm]	θ [º]
B1	12/2.12	1.4	15
B2	12/2.12	1.4	27
B3	12/2.12	1.4	39
B4	15/1.69	1.4	15
B5	15/1.69	1.4	27
B6	15/1.69	1.4	39
B7	18/1.41	1.4	15
B8	18/1.41	1.4	27
B9	18/1.41	1.4	39

4. DATA REDUCTION PROCEDURE

The ultimate objective of data reduction is to obtain the overall conductance UA and the overall heat transfer coefficient U in time. Basic data analysis includes determination of the capacity of the heat exchanger, which is calculated from both the refrigerant side and the air side balances, as shown by Eqs. (1) and (2):

$$q_r = \dot{m}_r C_{pr} (T_{r,out} - T_{r,in}) \quad (1)$$

and

$$q_a = \dot{m}_a (h_{a,in} - h_{a,out}) = q_{a,s} + q_{a,l,} \quad (2)$$

with

$$q_{a,s} = \dot{m}_a (C_{pa,in} T_{a,in} - C_{pa,out} T_{a,out}) \quad (2a)$$

$$q_{a,l} = q_a - q_{a,s} = \dot{m}_{fr} h_{sg} \quad (2b)$$

$$q = \frac{(q_r + q_a)}{2} \quad (3)$$

$$\Delta q = \frac{|q_r - q_a|}{q} \quad (4)$$

Two energy balances are used to verify proper operation for each test run. Equation (4) defines the difference between the two energy balances calculated for each data point. The difference in energy balances remained below 5% for all tests when approaching steady conditions.

The □-NTU method was used for obtaining overall heat transfer coefficient U. This equation applies to cross–flow HX, with both fluids unmixed (Kays and London, 1984).

$$\varepsilon = 1 - exp\left\{\frac{NTU^{0.22}}{C^*}[exp(-C^* NTU^{0.78}) - 1]\right\} \quad (5)$$

$$\varepsilon = q / q_{max} \quad (6)$$

$$q_{max} = (\dot{m}C_p)_{min} \times (T_{a,in} - T_{r,in}) \quad (7)$$

$$C^* = \frac{(\dot{m}C_p)_{min}}{(\dot{m}C_p)_{max}} \quad (8)$$

$$UA = (\dot{m}C_p)_{min} NTU \quad (9)$$

$$U = \frac{UA}{A} \quad (10)$$

5. RESULTS AND DISCUSSION

As mentioned, this paper presents is focused on the effect of the louver angle θ, as illustrated in Figure 3(b). Three louver angles are explored: 15º, 27º, and 39º where maximal performance is expected to be in the typical face flow velocities. Nine heat exchangers differing in the louver angle and fin pitch are presented of total of 15 originally studied to see geometric effects (see Table 2). In the test conducted to explore the effect of the louver angle on the performance of the heat exchanger (presented in this paper), louver pitch is kept constant (1.4 mm). All nine heat exchangers have the same louver pitch, face area, fin height, fin depth and were tested under the same conditions of inlet air temperature and relative humidity, refrigerant inlet temperature, and air and refrigerant mass flow rates (Tables 1 and 2).

It is important to understand the effect the louver angle has on the performance of the heat exchanger not only during frosting (first cycle), but also in refrosting conditions. Frosting is the growth of a frost layer on a clean, dry heat exchanger whereas refrosting is the growth of frost on a heat exchanger that has been defrosted and has water being retained on the surface of the fins. Refrosting is more common during heat exchanger operation since frosting only occurs when the heat exchanger is first installed or when all of the water from the melting frost layer after a defrost has been removed. Thus it is the most important for the operation of the heat exchanger in reality to understand the refrosting cycle that is repetitive – others are just transients.

5.1 The performance at the beginning of the first frosting cycle

5.1.1 Effect of louver angle on the initial pressure drop and overall heat transfer coefficient during the first frosting cycle

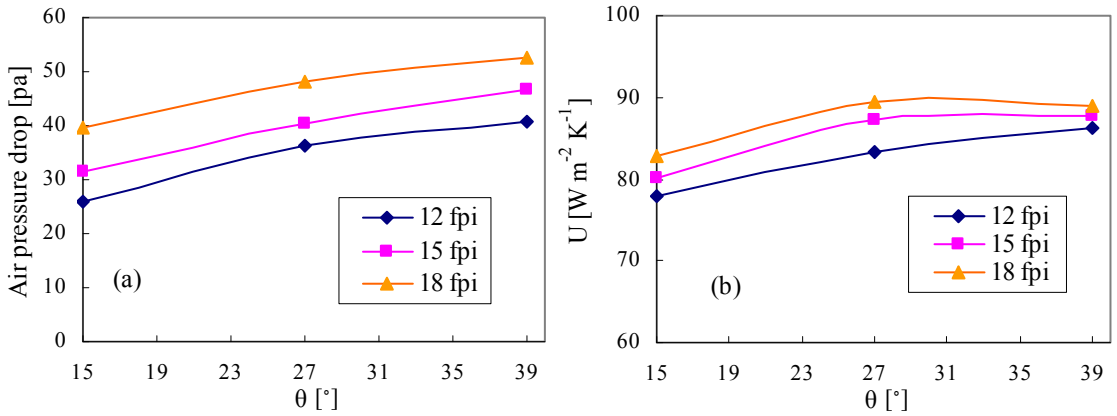

Fig. 4: Variations of air-side pressure drops and overall heat transfer coefficient with louver angle at the beginning of the first frosting cycle (clean surface) for three different fin pitches at face velocity: 3.5 m/s

Figure 4. presents the pressure drop data and overall heat transfer coefficient at the beginning of the first frosting cycle, for the multi-louvered fin heat exchangers with different louver angles, 15°, 27° and 39°, and the fin pitches, 12 fpi, 15 fpi, and 18 fpi (fin spacing 2.12, 1.41, and 1.69 mm). Even these tests were conducted at 80% relative humidity using the test conditions stated in Table 1., graphs indicate operation in dry condition. Pressure drop increases with louver angle for all fin pitches, but the gradient is reduced as louver angle increases (see Fig. 4(a)). For the fin with 18fpi the pressure drop at the beginning of the first frosting cycle for the louver angle 27° is about 21% higher than 15° and is about 8% lower than 39°.

The overall heat transfer coefficient increases with louver angle for small louver angle (louver angle less than 27° in this case), but for the greater louver angle its effect on the overall heat transfer coefficient varies with fin pitch, as

shown in Fig. 4(b). For 12 and 15 fpi, the overall heat transfer coefficient at the beginning of the first frosting cycle increases with louver angle but for Fp = 18 fpi, decreases with louver angle greater than 27°. This indicates that for given geometry and operating conditions maximum heat transfer performance occurs at around 27° louver angle. The overall heat transfer coefficient at the beginning of the first frosting cycle for louver angle 27° with fin pitch 18 fpi is about 0.7% higher than 39° and about 8 % higher than 15°. This may be due to the lower "flow efficiency", see Webb and Trauger (1991). As the low louver angle, some of the flow stream bypasses the louver passages and flows as "duct flow", between the fin channels. The heat exchanger performance is then close to that of a plain duct, and the louvers are relatively ineffective. As the louver angle increases, the friction factor and pressure drop along the duct flow path increase, causing more flow in the louver direction. Similarly, as the fin spacing decreases, the hydraulic resistance in the louver direction decreases with respect to the axial direction, so more of the flow will pass through the louver direction, which implies a higher "flow efficiency".
Figure 5 presents to scale drawings of three geometries with fin pitch 18 fpi and louver pitch 1.4 mm explored to facilitate understanding of the trends shown in Figure 4(b). It looks like at lower louver angle 15° geometry favors duct directed flow while at 39°geometry favors stronger louver directed flow. Structures with middle louver angle (27°) seem to be more balanced and that is what correlates well with the heat transfer performance as shown earlier.

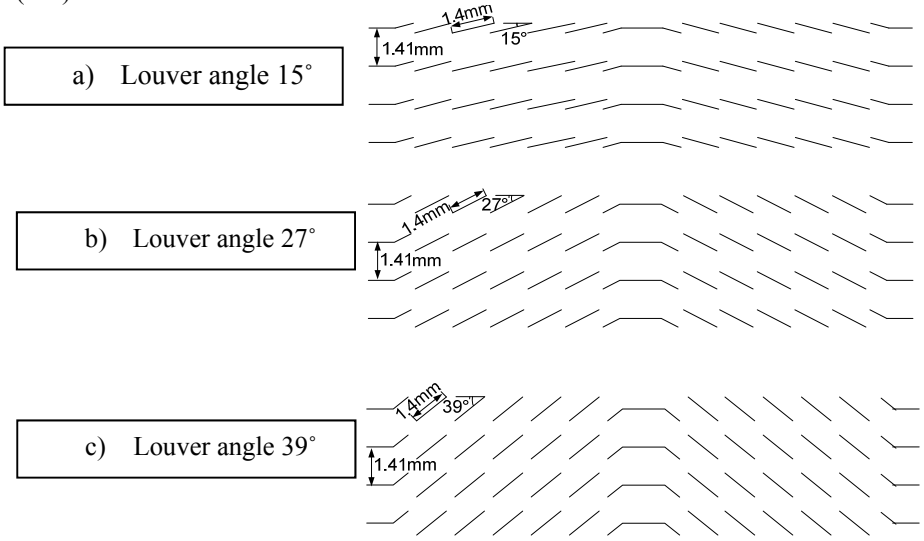

Fig. 5: Louvered-fin arrays for fin pitch 18 fpi (fin spacing 1.41mm), louver pitch 1.4 mm, louver angle 15˚, 27˚, 39˚

5.1.2 Effect of louver angle on initial Colburn f and Fanning friction j factors during the first frosting cycle and comparison to the prediction by the Chang and Wang (1997)
The data reduction process for the air-side convective heat transfer coefficient, ha, during the first frosting cycle, is the same as Xia et al. (2006), which is developed based on Xia and Jacobi (2004, 2005), and Zhang and Hrnjak (2010a), so only a brief description is given here.

$$\frac{q_{a,s}}{F\Delta T_{lm}} = \frac{1}{\eta_a h_a A_a} + \frac{1}{h_r A_r (q_{a,s}/q_a)} \tag{11}$$

$$\eta_a = \eta_f \frac{A_f}{A_a} + \left[\frac{k_{fr}/\delta_{fr}}{h_a(q_a/q_{a,s}) + k_{fr}/\delta_{fr}}\right]\frac{A_a - A_f}{A_a} \tag{12}$$

$$\eta_f = \frac{2\lambda}{h_a(q_a/q_{a,s})F_h\delta_{fr}} tanh\left(\frac{\lambda F_h}{2\delta_{fr}}\right)(k_f\delta_f/2 + k_{fr}\delta_{fr}) \tag{13}$$

with

$$\lambda = \delta_{fr}\sqrt{\frac{h_a(q_a/q_{a,s})}{k_f\delta_f/2 + \delta_{fr}[k_f h_a(q_a/q_{a,s})(\delta_f/2)/k_{fr} + k_{fr}]}} \tag{14}$$

Where ΔTlm is the log–mean temperature difference determined under the assumption of counter flow conditions, and F is the cross–flow correction factor to ΔTlm. The values for F are obtained using the plot of logarithmic–mean temperature difference correction factor for a cross–flow heat exchanger developed by Bowman et al. (1940).
For the initial value during the first frost-growth cycle, ηa,0 and ηf,0 can be expressed as following:

$$\eta_{a,0} = 1 - \frac{A_f}{A_a}(1-\eta_{f,0}) \tag{15}$$

$$\eta_{f,0} = \frac{tanh[\sqrt{2h_a(q_a/q_{a,s})/(k_f\delta_f)}(F_h/2)]}{\sqrt{2h_a(q_a/q_{a,s})/(k_f\delta_f)}(F_h/2)} \tag{16}$$

Flow inside the tube was laminar (400<Re<700) and the flat tube refrigerant-side heat transfer coefficient was determined based on the Shah correlation (1975). For RerPrrDr/TL ⩾ 33.3 (here in the range of 38< RerPrrDr/TL <55), that is:

$$Nu_r = 1.953\left(\mathrm{Re}_r\,\mathrm{Pr}_r\frac{D_r}{T_L}\right)^{1/3}\left(\frac{\mu_r}{\mu_w}\right)^{0.14} \tag{17}$$

Then, the refrigerant-side convective heat transfer coefficient is obtained by

$$h_r = \frac{Nu_r k_r}{D_r} \tag{18}$$

The heat transfer and pressure drop can be expressed in terms of the Colburn factor, j, and the Fanning friction factor, f. The air is treated as an incompressible fluid, and the density of air is treated as constant according to the average air temperature.

$$f = \frac{A_{ff}}{A_{tot}}\left(\frac{2dp}{\rho v^2}\right) \tag{19}$$

$$j = \frac{h_a}{GC_p}\mathrm{Pr}^{2/3} \tag{20}$$

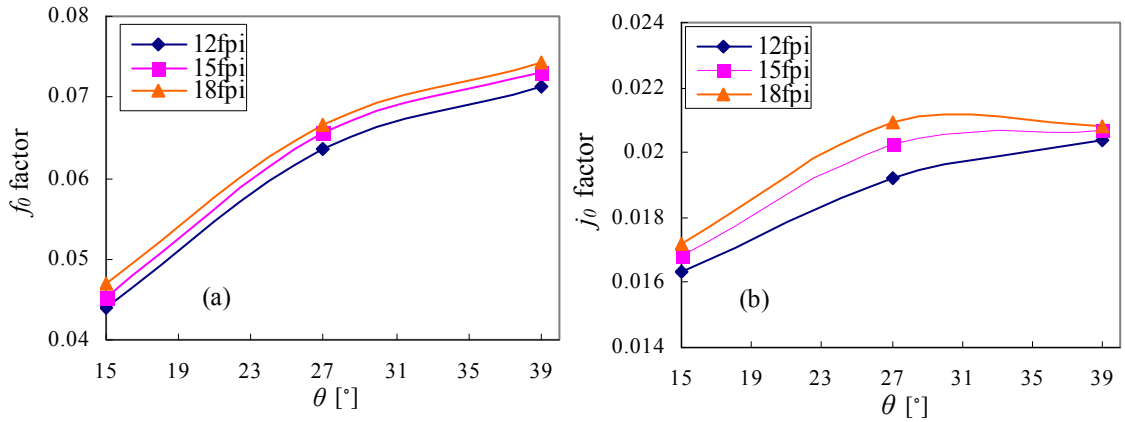

Fig. 6: Effect of louver angle j_0 and f_0 factors at the beginning of the first frosting cycle

Figure 6 displays the effects of louver angle on the initial Colburn j0 factor and the initial Fanning friction factor f0 during the first cycle. Figure 6(a) shows that the Fanning friction factor, f0, increases as the louver angle gets larger and the fin spacing gets smaller. Figure 6(b) shows that the j0 factors have the same trends as the initial overall heat transfer coefficient: for 12 and 15 fpi, the j0 factors increases with louver angle but for Fp=18 fpi, the j0 factors increases with louver angle when louver angle is less than 27°, and decreases with louver angle when louver angle is greater than 27°.

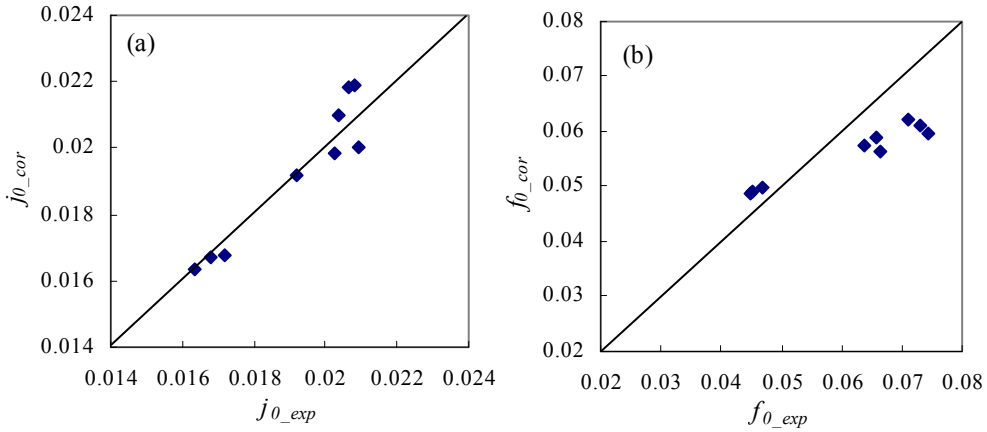

Fig. 7: Comparison of experimental data and correlations for the j_0 and f_0 factor

Figure 7 shows the comparison of experimental data and the prediction by Chang and Wang correlation (1994) for the j0 and f0 factors: experiments and the correlation are within 10% for j0.factors and 20% for f0 factors. The deviation is at very low levels and slightly increases with the louver angle. That indicates that this unique, one sided HX is a very good representation of operation of the fins of this kin in the real, complete heat exchanger, or that effect of slightly reduced fin efficiency is in the noise.

5.2 The performance in frosting

5.2.1 Effect of louver angle on air-side pressure drop

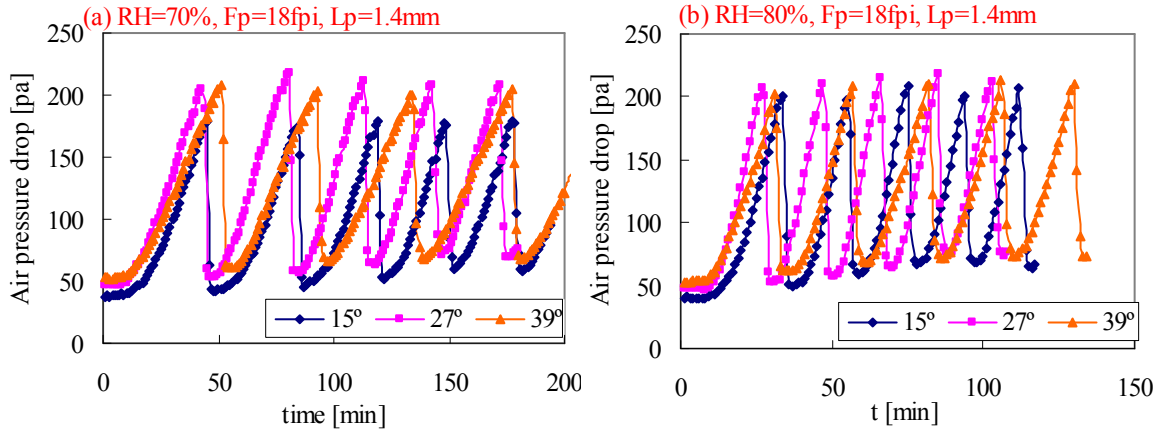

Figure 8: Effect of relative humidity on the air-side pressure drop for heat exchangers with louver angle 15°, 27° and 39° for the fin pitch 18fpi during the first five frosting periods, face velocity: 3.5m/s

Effect of relative humidity of inlet air (here 70% and 80%) on air side pressure drop is shown in Fig. 8. for the multi-louvered fin with different louver angles, 15°, 27° and 39°, for the fin pitch18 fpi during the first five frosting periods. As expected, the pressure drop at the beginning of each cycle increases in first four cycles due to retention of the water after defrost that was in a quantity sufficient to be retained, not drained. This is due to a greater water retention capability on the surface of the fins compared to a relatively small quantity of frost between fins because low frost density. The surface could retain water from multiple frosting periods. The water retained blocks the flow and thus increases the pressure drop across the heat exchanger. Even more, the water acts as a parasitic thermal mass because it changes phase in each frost/defrost cycle. It takes four to five cycles to accumulate water to its limit and the drain will start. That will result in unchanged value of pressure drop at the beginning of each refrost cycle. This phenomenon was visually confirmed by photographs that were taken during the tests and will be explained later in the paper. More on this issue can be found in Zhang and Hrnjak (2010a) which shows that in some cases it is needed seven to eight cycles to come to a steady state condition.

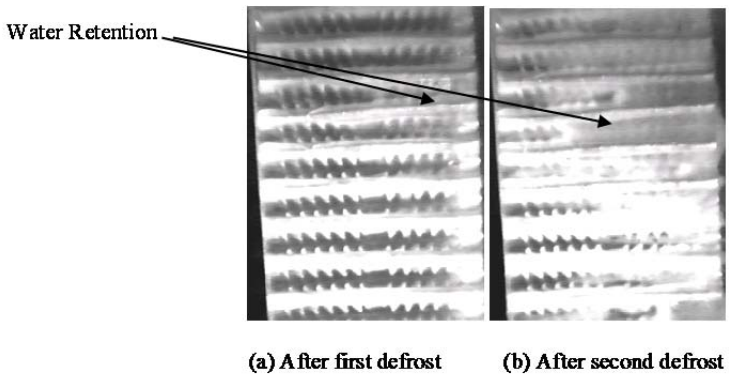

Figure 9: Visual observation of water retention after the first and second refrosting periods.

Figure 9 on the left depicts water retention on the surface of the fins after the first defrosting period. This explains the increase in the pressure drop at the beginning the first refrosting period. The picture of the fins after the second defrost (on the right) shows that there is more water on the surface of the fins than in the first defrosting period. This is due to the additional water from the frost that was melted during the second defrost, but has not been removed. This explains the increase in the pressure drop at the beginning of the second refrosting period when compared with the pressure drop at the beginning of the first refrosting period.

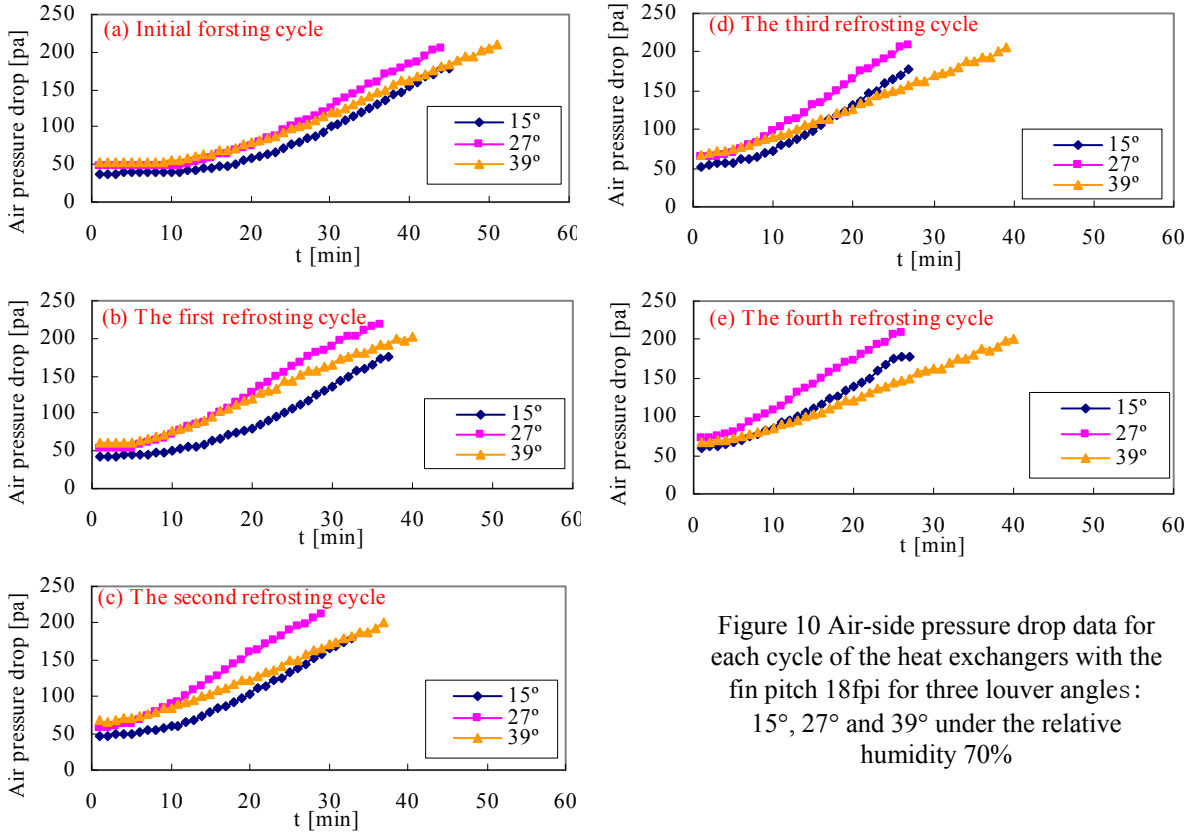

Figure 10 Air-side pressure drop data for each cycle of the heat exchangers with the fin pitch 18fpi for three louver angles: 15°, 27° and 39° under the relative humidity 70%

Figure 10 shows details of the pressure drop progression in Figure 8(a) for heat exchangers with 18 fpi and louver angles: 15°, 27° and 39°, by aligning all cycles to start from the zero time. Figure 10(a) compares the pressure drops during the initial frosting period. At the beginning of the frost accumulation period, heat exchangers with larger louver angles have higher pressure drop. As time progresses to near the point where defrosting is necessary, the fin with 39° louver angle has nearly the same pressure drop as the 27° case. The heat exchanger with a fin with a louver angle of 15° has the lowest pressure drop, probably because duct directed flow is far less affected by frost bridging

the louvers (see Fig. 5.). The operational (refrigerating) time, which is a consequence of the defrost criterion of five times increase compared to dry pressure drop, is longest for the fin with 39° louver angle.
Figure 10(b) shows the pressure drops in the first refrosting period. The 39° louver angle specimen still has the highest pressure drop at the beginning of the first refrosting period, but the 27° specimen degrades more quickly.

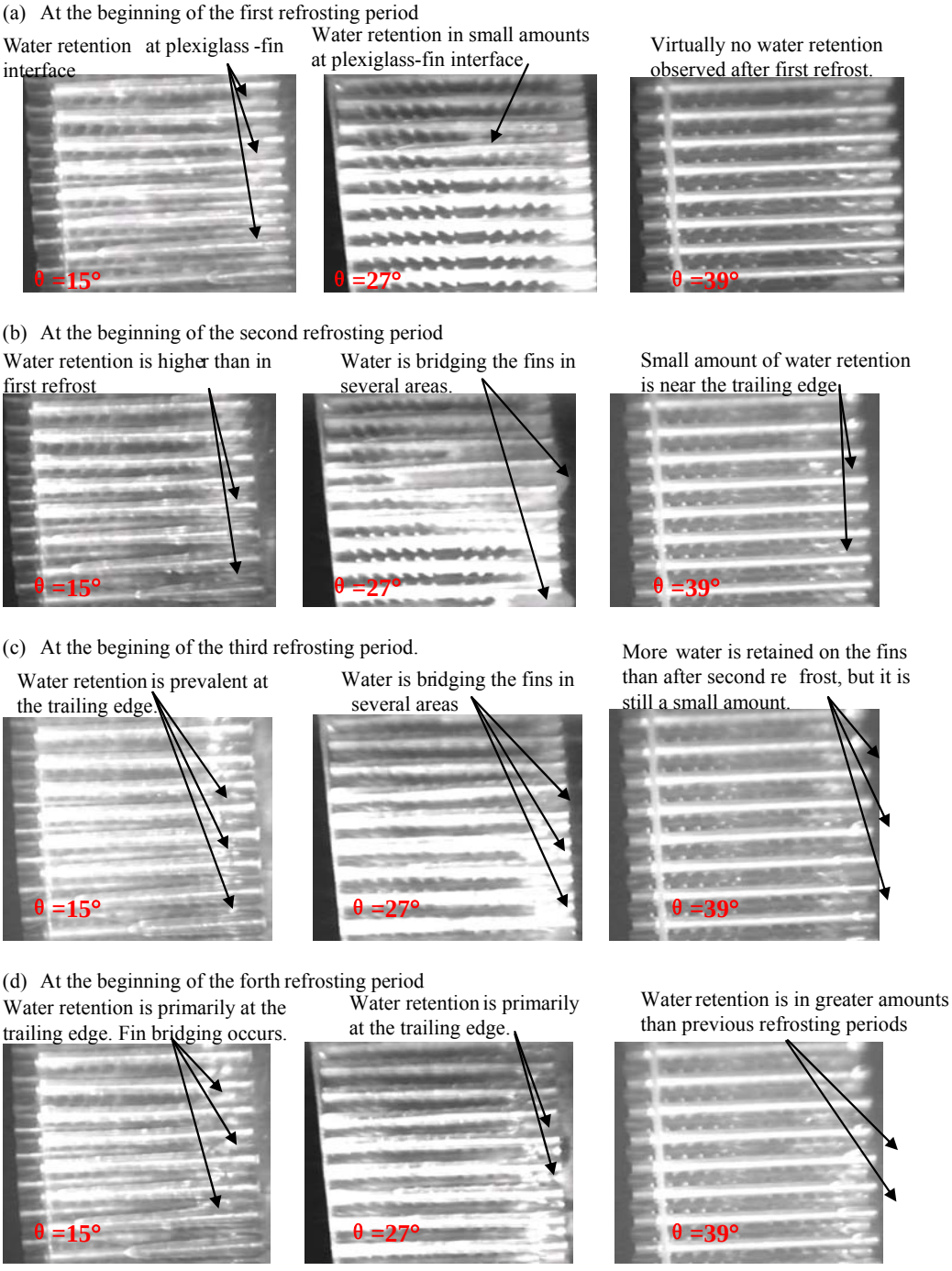

Figure 11: Heat exchangers with fin pitch 18fpi and louver angle 15°, 27° and 39° at beginning of refrost

Figure 11 shows the water retention on the surface of the fins after each defrost for heat exchangers with 18 fpi and louver angles, 15°, 27° and 39°. Figure 11(a) shows that all heat exchangers retain water, but in moderate amounts

at the beginning of the first refrosting period. Heat exchanger with 39° has virtually no water retention observed on the fin surfaces. Heat exchanger with 27° had water at the plexiglass-fin interface in smaller amounts than heat exchanger with 15°. That valley represents location of the tube where condensate or water after defrost tends to stay. This situation could be explained by easier retention/bridging in the smaller louver angled heat exchangers.

There are two primary paths of water removal in HXs with vertically oriented tubes and they were clearly visible in the experiment illustrated in Figure 12. The first path is through the louvers, where the water flows downwards, along the louver edge, then moves to the upper part of the lower below, and again downwards following the louver and son, due to the force of gravity. Overall movement is down. The mas flux of water increases towards the bottom. The other path is in the airflow direction towards the trailing edge of the fin due to the shear force from the air. This direction generally does not result in water removal unless blow-off (carry-over) occurs or special provisions are made.

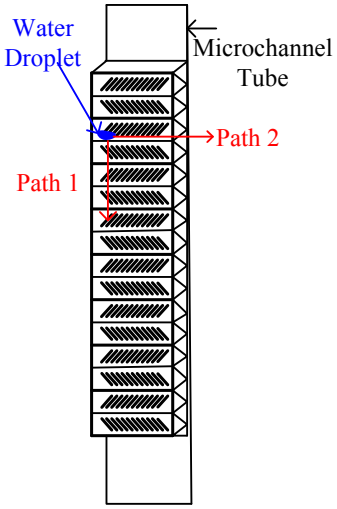

Figure 12: Illustration of water movement and removal modes.

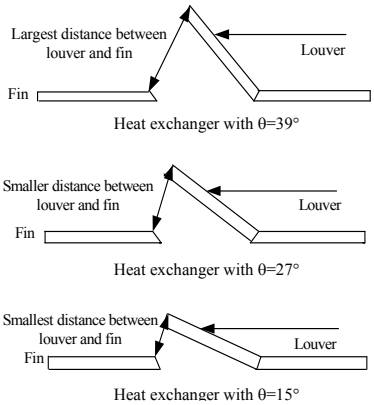

Figure 13: Drawings illustrating the impact of the louver angle on the channel area that is available for water to flow.

Needless to say water removal is very important since the larger amount of water retained on the fins bridges the louvers turning "louver directed" into a "duct directed" flow, blocks the airflow and once heat exchanger is turned to refrigeration mode, the water freezes and stays on the surface of the fins. The ice plugs can also bridge the louvers, which also causes the flow to change from louver directed flow to duct directed flow. In addition, This takes away the heat transfer enhancement provided by the louvers. When non-stiff blowers are used, it will drastically decrease the air mass flow rate. Also, the ice acts as additional thermal resistance to heat transfer thus causing a decrease in capacity. Needless to say it takes energy to turn the water retained into the ice and to melt it in defrost. It was seen that once a droplet is created it stays for several cycles sometimes even not melting in defrost, until finally grows so big that it is moved by air.

Figure 13 illustrates the effect that the louver angle has on the flow of water through the louvers. When the louver angle is large, the distance and corresponding area between the louver and the fin is larger than when the louver angle is small, when other louver geometrical parameters are held constant. Thus, it is less likely for water to get caught up or bridge the louvers. This is important since having water flow from upper fins to lower fins and thus, water flows down the heat exchanger more freely for heat exchanger with 39° than the other two heat exchangers.

Thus the water flowed to lower portions of the heat exchanger. This is important since this leaves the top portion of the heat exchanger with small amounts of water retention.

Figure 10(c) confirms that observation: the heat exchanger with 39° is able to run for a much longer operating time (up to 50%) than the other two heat exchangers and has a similar pressure drop as 15°.. There is also a noticeable increase in the pressure drop at the beginning of the frosting which indicates that all of the heat exchangers have retained more water than in the previous period. Heat exchanger with 27° has the worst pressure drop profile (the most sensitive to frost) by the time the defrosting criterion is met.

Photographs presenting water retention at the beginning of the second refrosting period are in Figure 11(b). It is again shown that heat exchanger with 39° has the smallest amount of water retained in the area where the pictures are taken. The reason for this behavior was described above. All three heat exchangers have greater amounts of

water retention in the viewable area than in the previous refrost cycle. It is also important to note that when bridging occurs, it typically happens at or near the trailing edge due to the air flow pushing greater amounts of water towards the exit.

The pressure drop in the third refrost are shown in Figure 10(d). The trends are the same as in the previous cycle. This is again due to additional water being retained on the surface of the heat exchangers. The heat exchanger with the smallest louver angle again has the smallest pressure drop at the beginning of the refrosting period, but it degrades much more quickly when compared to heat exchanger with 39°. Heat exchangers with 27° and 39° have nearly identical pressure drop at the beginning of the third refrosting period.

Photographs after the third defrost are shown in Figure 11(c). Again it appears that water drainage is better in fins with a larger louver angle. Water accumulates in larger quantities near the trailing edge of the heat exchanger.

The pressure drops in the fourth refrosting period are plotted in Figure 10(e). Situation is the same as in previous cycle, just expanded.

Photographs at the beginning of the fourth refrosting period and are shown in Figure 11(d). It appears that the area where the pictures were taken is nearly saturated -water bridged the fins near the trailing edge for heat exchangers with louver angel 15° and 27°.

Thus, comparison of the pressure drop characteristics under the cyclical frosting conditions, after several refrosting cycles, the heat exchanger with the largest louver angle had the most desirable pressure drop characteristic due to the best drainage.

5.2.2 Effect of louver angle on overall heat transfer coefficient

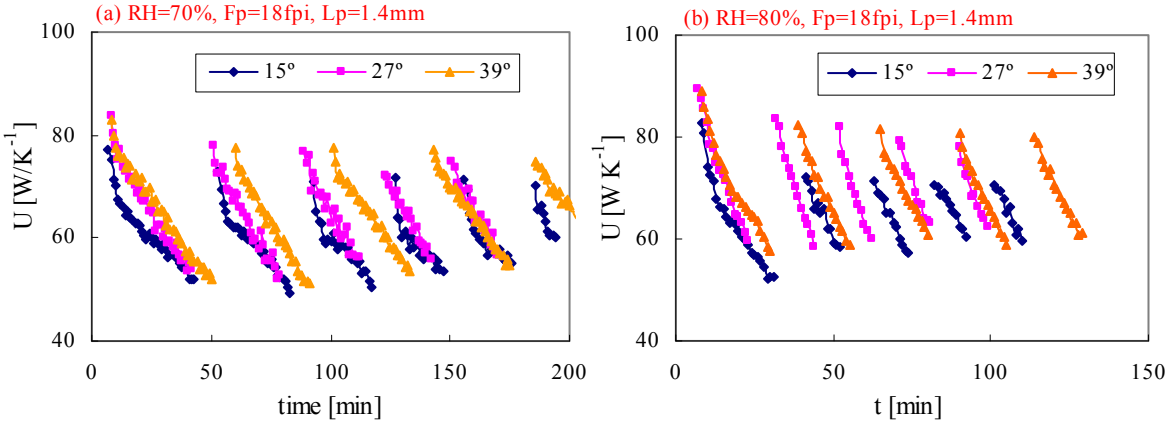

Figure 14: Effect of humidity on overall heat transfer coefficient for heat exchangers with louver angle 15°, 27° and 39° for the fin pitch 18fpi heat exchanger during the first five frosting periods

The overall heat transfer coefficient characteristics for the multi-louvered fin heat exchangers with different louvered fin geometries are presented in Fig. 14 for two air humidities and five cycles. Figure 15 shows the details of the process in Figure 14. Figure 15(a) shows that the heat exchanger with 27° has the highest heat transfer coefficient during the beginning period of the first (and later every) frosting cycle. The overall heat transfer coefficient with the smallest louver angle (15°) has the lowest overall heat transfer coefficient throughout the tests. It is not a surprise when looking in the information in the Figure 5, and also Fig. 6(b). Nevertheless the louver angle of 27° has a larger decrease in performance than the louver angles of 39°, both in each cycle and in each consecutive cycle. Another important characteristic is significant drop in heat transfer coefficient in the frosting cycle (while doing the job): form initial values around 90 Wm-2s-1 It drops to around 60 Wm-2s-1 before defrost.

The first refrosting period was initiated immediately after the first defrosting period was terminated (2min). Once the frost layer had melted completely to water, refrigerant was once again allowed to flow through the heat exchangers and thus the cooling period started. The overall heat transfer coefficients during the first refrosting period for these three heat exchangers were determined and are shown in Figure 15(b). All three heat exchangers show a slight decrease in the overall heat transfer coefficient at the beginning of the frosting period in each consecutive cycle until reaching the steady value. It appears that it is due to slight increase in water retained on the fin surfaces. The water acts as an additional thermal resistance to heat transfer and may affect the air flow through the fin/louver structure. Nevertheless, the impact of water retention on the heat transfer coefficient appears to be very small. Comparison of three louver angles show the same order: the heat exchanger with 27° has the highest heat transfer coefficient (but not for much) during the beginning period of the first refrosting cycle but it has a larger

decrease in performance than the louver angles of 15° and 39°. The heat exchanger with the smallest louver angle (15°) has the lowest heat transfer coefficient throughout the tests.

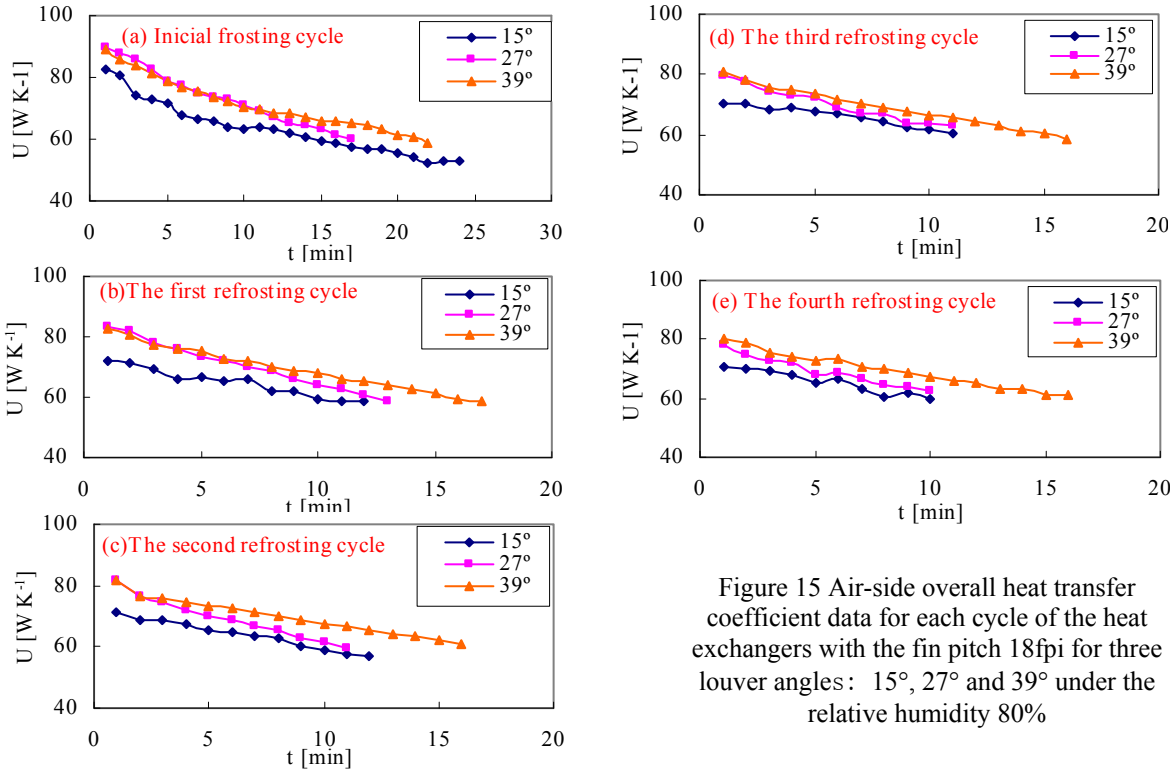

Figure 15 Air-side overall heat transfer coefficient data for each cycle of the heat exchangers with the fin pitch 18fpi for three louver angles: 15°, 27° and 39° under the relative humidity 80%

Figure 15(c) shows the situation in the second refrost. The major difference is development of the 39o louver as the best performer, due to: the highest heat transfer coefficient, the least reduced heat transfer coefficient in frosting, and the longest operation in frosting.

Again, during the third refrost, there is a slight, minimal decrease in the overall heat transfer coefficients when compared to the previous refrosting period (Figure 15(d)). This is due to additional water being retained by the heat exchangers. The trend appears that the heat exchangers with larger louver angles have higher overall heat transfer coefficients throughout.

The situation after the fourth defrost is shown in Figures 15(e). The same trends as the third refrosting periods are observed. Again, the overall heat transfer coefficient is higher for larger louver angles. The steady operation seems to have been reached.

Thus, comparison of the performance characteristics (pressure drop and overall heat transfer coefficient) under the cyclical frosting conditions indicate that the heat exchanger with louver angle of the fin 39° has the best overall characteristics (for 18 fpi and 3.5 m/s face velocity). It is because the performance in the fully repetitive conditions (after initial 3-5 refrosting cycles) is what matters for actual operation, even 27° angle has the highest overall heat transfer coefficient during the first few cycles, or the 15° heat exchanger has the lowest pressure drop.

5. SUMMARY AND CONCLUSIONS

This paper presents the results of an experimental investigation of the performance of serpentine-louvered-fin, microchannel heat exchangers in periodic frosting. The focus is on the effect of louver angles: 15°, 27° and 39° for the three fin pitches (12, 15 and 18fpi) on pressure drop and overall heat transfer coefficient.

When searching for good design typically higher heat transfer is accompanied with higher pressure drop and the selection of a good combination is a function of the application. In the case of operation in frosting designer could also ask: would the good performing geometry in dry conditions still be good in frosting. Results presented in the paper indicate important trend in that respect: the combination that was not good in dry condition (39° and 18fpi in Fig. 4) turned to be very good in frosting (Figs. 10 and 15). Even more important is the fact that the difference shows more and more prominent in later consecutive frosting cycles. These operations (numerous consecutive frosting – refrosting cycles) are the most typical for real operating situations and are typically neglected in studies of

frosting. In other words: CONCLUSIONS FROM DRY TEST AND EVEN FIRST TWO THREE REFROSTING CYCLES DO NOT HOLD IN REAL OPERATION WHERE MULTIPLE CONSECUTIVE FROSTING OCCURS.
It is found that the pressure drop at the beginning of the first frosting cycle (clean operation) for all fin pitches increases with louver angle, but the effect of louver angle on the pressure drop decreases for louver angle larger than 27°. For the fin with 18 fpi the pressure drop at the beginning of the first frosting cycle for the louver angle 27° is about 21% higher than 15° and for louver angle 27° is about 8% lower than 39°.
Comparing the results from the tests run on the specimens with three louver angles, 15°, 27° and 39°, for the three fin pitches, 12 fpi, 15 fpi, and 18 fpi, (again I do not see two other fin pitches: 12 and 15) the overall heat exchanger coefficient, at the beginning of the first frosting cycle, increases with louver angle for small louver angle (louver angle less than 27° in this case), but for the greater louver angle its effect on the overall heat exchanger coefficient varies with fin pitch. For Fp=12 fpi, the overall heat exchanger coefficient at the beginning of the first frosting cycle increases with louver angle. For Fp=18fpi, the overall heat exchanger coefficient at the beginning of the first frosting cycle increases with louver angle when louver angle is less than 27°, and decreases with louver angle when louver angle is greater than 27°. The overall heat transfer coefficient at the beginning of the first frosting cycle for louver angle 27° with fin pitch 18 fpi is about 0.7% higher than 39° and about 8 % higher than 15°.
Several (here typically four) repetitive defrost cycles were needed to reach saturation in water retention. Each heat exchanger had an increase in the pressure drop at the beginning of first four consecutive refrosting periods due to excess water being retained. For the fin pitch 18 fpi, after several refrosting cycles, the heat exchanger with the largest louver angle had the highest overall heat transfer coefficient throughout and had the most desirable pressure drop due to the best drainage.
The photos show that the heat exchanger with the largest louver angle had the least amount of water in the visible region. Thus, the geometry with larger louver angle was able to drain the water down the heat exchanger more efficiently. As water drains downward, it fills areas that are more susceptible for the water to be retained in, but it also goes to areas that drain more easily. When large quantities of water are present, it is easier for the water to be removed off of the heat exchanger by the airflow pushing the water off of the trailing edge. Thus, the conclusion from these tests were that the heat exchanger with the largest louver angle had the most desirable behavior after several refrosting periods with respect to both the overall heat transfer coefficient, pressure drop, and water movement.
This conclusion is very important because it shows shortcomings of the choices based on the only one frosting period, typical for many studies in this field. The selection of the high angle louver would not have been justifiably made based on the results of the first cycle.

NOMENCLATURE

A	area (m^2)	h_{sg}	latent heat of ablimation (for water vapor) ($J\ kg^{-1}$)	T_s	tube spacing (on centers) (mm)
C_P	specific heat ($J\ kg^{-1}\ K^{-1}$)	j	Colburn factor (-)	t	time (min)
D	hydraulic diameter (m)	k	thermal conduct. ($Wm^{-1}\ °C^{-1}$)	U	overall heat transfer coefficient ($W\ K^{-1}\ m^{-2}$)
D_{avg}	average deviation (%)	L_p	louver pitch (mm)	UA	overall conductance ($W\ K^{-1}$)
D_{mean}	mean deviation (%)	$\dot{m}$	mass flow rate ($kg\ s^{-1}$)	x	the data element (-)
dP	pressure drop (kPa)	Nu	Nusselt number (-)	ΔT_{lm}	log-mean temperature difference (°C)
F	cross-flow correction factor (-)	Pr	Prandtl number (-)	δ	thickness (m)
F_d	fin depth (mm)	q	heat transfer rate (W)	ϕ	relative humidity (%)
F_h	fin height (mm)	Re	Reynolds number based on hydraulic diameter (-)	η_a	overall surface efficiency (-)
F_p	fin pitch (fpi)	Re_{Lp}	air side Reynolds number based on louver pitch (-)	η_f	frosted-fin efficiency (-)
F_s	fin spacing (on centers) (mm)	T	temperature (°C or K)	μ	viscosity of fluid (Pa-s)
f	friction factor (-)	T_L	Tube length (m)	θ	louver angle
G	air-flow mass vel. ($kg\ m^{-2}\ s^{-1}$)	T_{major}	tube major (mm)	ρ	density ($kg\ m^{-3}$)
h	convective heat transfer coefficient ($W\ m^{-2}\ °C^{-1}$)	T_{minor}	tube minor (mm)	υ	air velocity between fins ($m\ s^{-1}$)

Subscripts

0	initial value
cor	by correlation
d	defrost
dp	dew-point
exp	by experiment
f	fin
ff	free-flow
fr	frost
in	inlet
l	latent heat
n	nozzle
out	outlet
r	refrigerant (or refrigerant side)
s	sensible heat
tot	total friction
w	wall
a	moist air (or air side)

REFERENCES

Balekjian, G., Katz, D., Heat transfer from superheated vapors to a horizontal tube, *A.I.Ch.E. J.*, 4 (1) 1958, pp. 43-48.

Achaichia A, Cowell T. A., 1988. Heat transfer and flow friction characteristics of flat tube and louvered plate fin surfaces. Exp. Thermal Fluid Sci. Vol. 1; p. 147-157.

Bowman, R.A., Mueller, A.C., Nagle, W.M., 1940. Mean temperature difference in design. Trans. ASME 62, 283–294.

Carlson, D. M., Hrnjak, P. S., and Bullard, C. W., 2001. Deposition, distribution, and effects of frost on a multi-row heat exchanger performance. Department of Mechanical and Industrial Engineering. Urbana, University of Illinois, ACRC TR-183.

Kim J, Groll E.A., 2003. Performance comparisons of a unitary split system using microchannel and fin-tube out-door coils. ASHRAE Transactions, 109(2), p. 219-229.

Kondepudi S. N, O'Neal D. L., 1987. The Effect of frost growth on extended surface heat exchanger performance － a Review. ASHRAE Transactions 93(2), 258-274.

Kondepudi S. N, O'Neal D. L., 1989. The Effect of frost growth on the performance of louvered finned tube heat exchangers. International Journal of Refrigeration. 12, P. 151-158.

Machielsen, C.H.M., Kerschbaumer, H.G., 1989. Influence of frost formation and defrosting on the performance of air coolers: standards and dimensionless coefficients for the system designer. Int. J. Refrigeration 12, 283–290.

Webb, R.& P. Trauger, 1991. Flow structure in the louvered fin heat exchanger geometry. Exp. Therm. Fluid Sci, 4; P. 205-217.

Sankar Padhmanabhan, Lorenzo Cremaschi, Daniel Fisher, John Knight., 2008. Comparison of frost and defrost performance between microchannel coil and fin-and-tube coil for heat pump system. Proceedings of the 2008 International Refrigeration and Air Conditioning Conference at Purdue, Vol. I, p. 249-256.

Shah, R.K., 1975. Thermal entry length solutions for circular tube and parallel plates. In: Proc. 3rd National heat mass transfer conference, Indian Inst. Technology, Bombay, vol. 1, HTM-11-75.

Kays W. M. and A. L. London. (1984). Compact Heat Exchangers, 3rd Ed. New York: McGraw-Hill Book Company.

Yan, W. M. , H. Y. Li and Y. L. Tsay, 2005. Thermofluid characteristics of frosted finned-tube heat exchnagers, Int. J. Heat Mass Transfer, 48, P. 3073-3080.

Xia, Y., Jacobi, A.M., 2004. An exact solution to steady heat conduction in a two-dimensional slab on a one-dimensional fin: application to frosted heat exchangers. Int. J. Heat Mass Transf. 47, 3317–3326.

Xia, Y., Jacobi, A.M., 2005. Air-side data interpretation and performance analysis for heat exchangers with simultaneous heat and mass transfer: wet and frosted surfaces. Int. J. Heat Mass Transf. 48, 5089–5102.

Xia Y, Y. Zhong, P. S. Hrnjak, and A. M. Jacobi, 2006. Frost, defrost, and refrost and its impact on the air-side thermal-hydraulic performance of louvered-fin, flat tube heat exchanger. Inernational Journal of Refrigeration, 29:7, 1066-1079.

Y.J. Chang, C.C. Wang, 1994. A generalized heat transfer correlation for louver fin geometry, Int. J. of Heat and Mass Transfer 40 (3), 533–544.

Zhang, P. and P. S. Hrnjak, 2009. Air-side performance evaluation of three types of heat exchangers in dry, wet and periodic frosting conditions. International Journal of Refrigeration, Vol. 32, p. 911-921.

Zhang, P. and P. S. Hrnjak, 2010. Effect of some geometric parameters on performance of PF2 heat exchangers in periodic frosting, International Journal of Refrigeration,Vol. 33, p. 334-346.

Zhang, P. and P. S. Hrnjak, 2010. Air-side performance of a parallel-flow parallel-fin (PF2) heat exchanger in sequential frosting, International Journal of Refrigeration, Vol. 33, p. 1118-1128.

ACKNOWLEDGEMENT

We are grateful for financial and technical support from Modine Manufacturing Company and for technical support from the Air Conditioning and Refrigeration Center (ACRC) at the University of Illinois.